Investigation of solution-processed bismuth-niobium-oxide films

Satoshi Inoue,[1,2,a)] Tomoki Ariga,[1,3] Shin Matsumoto,[2] Masatoshi Onoue,[3] Takaaki Miyasako,[3] Eisuke Tokumitsu,[1,2,3] Norimichi Chinone,[4] Yasuo Cho,[4] and Tatsuya Shimoda[1,2,3]

[1]*Green Device Research Center, Japan Advanced Institute of Science and Technology (JAIST), 2-13 Asahidai, Nomi, Ishikawa 923-1211, Japan*
[2]*School of Material Science, Japan Advanced Institute of Science and Technology (JAIST), 1-1 Asahidai, Nomi, Ishikawa 923-1292, Japan*
[3]*ERATO Shimoda Nano-Liquid Process Project, Japan Science and Technology Agency (JST), 2-13 Asahidai, Nomi, Ishikawa 923-1211, Japan*
[4]*Research Institute of Electrical Communication, Tohoku University, 2-1-1 Katahira, Aoba-ku, Sendai, Miyagi 980-8577, Japan*

(Received 4 August 2014; accepted 5 October 2014; published online 17 October 2014)

The characteristics of bismuth-niobium-oxide (BNO) films prepared using a solution process were investigated. The BNO film annealed at 550 °C involving three phases: an amorphous phase, Bi_3NbO_7 fluorite microcrystals, and Nb-rich cubic pyrochlore microcrystals. The cubic pyrochlore structure, which was the main phase in this film, has not previously been reported in BNO films. The relative dielectric constant of the BNO film was approximately 140, which is much higher than that of a corresponding film prepared using a conventional vacuum sputtering process. Notably, the cubic pyrochlore microcrystals disappeared with increasing annealing temperature and were replaced with triclinic β-$BiNbO_4$ crystals at 590 °C. The relative dielectric constant also decreased with increasing annealing temperature. Therefore, the high relative dielectric constant of the BNO film annealed at 550 °C is thought to result from the BNO cubic pyrochlore structure. In addition, the BNO films annealed at 500 °C contained approximately 6.5 atm. % carbon, which was lost at approximately 550 °C. This result suggests that the carbon in the BNO film played an important role in the formation of the cubic pyrochlore structure. © *2014 AIP Publishing LLC*.
[http://dx.doi.org/10.1063/1.4898323]

I. INTRODUCTION

Printed electronics technology has attracted considerable attention as a means for reducing the energy required for and the cost of fabrication of electronic devices such as large scale integrations, capacitors, and displays.[1–3] The critical aspects of printed electronics include the functional liquid materials and printing techniques used for their production. In particular, materials for insulators and dielectric films are indispensable in electronic devices. The bismuth-niobium-oxide (BNO) system is an attractive candidate for these applications,[4] because it has high relative dielectric constant (εr) and loss tangent ($\tan\delta$). Although several reports on bismuth-zinc-niobium-oxide films prepared using solution processes have appeared in the literature,[5,6] studies of BNO films are rare. One related example is the preparation of β-$BiNbO_4$ powder via a citrate sol-gel technique.[7]

Therefore, we developed a BNO precursor solution for the direct deposition of BNO films onto substrates using a solution process and investigated the characteristics of these BNO films, which were intended for use as insulators and dielectric films in electronic devices. We found that the BNO film annealed at 550 °C exhibited a high relative dielectric constant compared with that of a BNO film formed by a sputtering process. We also confirmed that cubic pyrochlore microcrystals appeared in the BNO films prepared using the solution process.[8] The strong relationship between the appearance of the cubic pyrochlore microcrystals and the remaining carbon in the BNO film was also investigated.

II. EXPERIMENTAL

A. BNO precursor solution

The BNO precursor solution was synthesized as follows. A 0.2 mol/kg bismuth solution (Bi-solution-1) was prepared by diluting a bismuth 2-ethylhexanoate (Bi-2EH) solution [Bi $(C_8H_{15}O_2)_3$ in 2-ethylhexanoic acid, Bi content: 25 wt. %, Wako] with 1-butanol (Bu-OH). Separately, a 0.2 mol/kg bismuth solution (Bi-solution-2) was prepared by diluting the Bi-2EH solution with 2-methoxyethanol (2ME). Next, a 0.2 mol/kg niobium solution (Nb-solution-1) was prepared by diluting a niobium 2-ethylhexanoate (Nb-2EH) [Nb $(C_8H_{15}O_2)_5$, 95% purity, Gelest] with Bu-OH. A 0.2 mol/kg niobium solution (Nb-solution-2) was also prepared by diluting Nb-2EH with 2ME. These solutions (Bi-solution-1, Bi-solution-2, Nb-solution-1, and Nb-solution-2) were each stirred at 1000 rpm and 110 °C for 20 min and then filtered through a 0.2–μm syringe filter [poly(tetrafluoroethylene), GE]. Next, Bi-solution-3 was prepared by mixing Bi-solution-1 and Bi-solution-2 in a 2:1 ratio. Nb-solution-3 was also prepared by mixing Nb-solution-1 and Nb-solution-2 in a 2:1 radio. Finally, Bi-solution-3 and

a)Author to whom correspondence should be addressed. Electronic mail: s-inoue@jaist.ac.jp.

Nb-solution-3 were mixed in a 1:1 ratio to provide the 0.2 mol/kg BNO precursor solution.

B. BNO film and capacitor fabrication

The BNO films were deposited on $Pt/TiO_x/SiO_2/Si$ substrates using the solution process. The thicknesses of the platinum and titanium oxide layers were 200 nm and 20 nm, respectively. After O_2 plasma cleaning using an FA-1 system (SAMCO), the BNO precursor solution was spin-coated on the substrate at 1500 rpm for 30 s, and then the substrate with the applied precursor solution was dried on a hot plate for 5 min at 250 °C. During this drying process, the BNO solution changed from a liquid to a gel state. This procedure was repeated five times to obtain a thick film. The film was then sintered in an O_2 atmosphere using a rapid thermal annealing system. The standard sintering conditions were 550 °C/20 min, and the thickness of the BNO film after sintering was approximately 170 nm. Next, 200-nm-thick Pt top electrodes were deposited using a mask sputtering method at 75 W. Finally, post annealing was performed to improve the adhesion between the top electrodes and BNO film. The annealing conditions were the same as those for sintering. The total annealing time was 40 min, i.e., 20 min each for the sintering and post annealing step, in this standard process.

C. Film characterization

The BNO film thicknesses were determined using a spectroscopic ellipsometer (SEMILAB Sopra GES5E). The Cauchy model was used to fit the data from 1.00 eV to 3.00 eV. Each top electrode area was measured using an MX50 microscope, DP25 digital camera, and DP2-BSW application software (Olympus) to accurately determine the electrode area. The capacitance of each BNO capacitor was determined using an SI1260 + 1296 Impedance/Gain-Phase Analyzer (Toyo) at a measurement frequency of 1 kHz and supplied voltages of 0 V and 0.1 V for the DC and AC biases, respectively. The relative dielectric constants were calculated using the measured thickness, top electrode area, and capacitance for each film. The thermal behavior of the BNO precursor solution was evaluated via thermal gravimetry differential thermal analysis (TG-DTA) using a TG/DTA-6200 (SII Nano Technology). X-ray diffraction (XRD) analysis was performed using an X'pert-Pro (PANalytical) at 45 keV and 40 mA. Cross-sectional, high-resolution transmission electron microscopy (HRTEM) images, selected-area electron diffraction (SAED) patterns, and nanobeam electron diffraction (NBD) patterns were obtained using a JEM-2011F microscope (JEOL). The composition of the BNO films was analyzed using a JED-2300T EDX system (JEOL). The surface roughness of the BNO films was analyzed using an atomic forth microscopy (AFM) and the dielectric constant in a film was measured using a scanning nonlinear dielectric microscopy (SNDM).[9] The SNDM method can detect changes in the dielectric constant in a film with changes in the oscillating frequency. Thermal desorption spectrometry (TDS) analysis was used to investigate the structural modification of the BNO films by annealing. The atomic ratios of oxygen, hydrogen, and carbon in the BNO films were determined via Rutherford backscattering spectrometry, hydrogen forward scattering spectrometry, and nuclear reaction analysis.[10]

III. RESULTS AND DISCUSSION

Figure 1 shows the results of the TG-DTA analysis of the BNO precursor solution in air atmosphere. First, a significant weight loss and an endothermic peak were observed at approximately 90 °C. This weight loss corresponded to the evaporation of the solvents, and the BNO solution transformed to a gel state. An exothermic peak then appeared at approximately 290 °C, which was attributed to the pyrolysis of the BNO gel, during which by-product molecules were evaporated, leading to a minor weight loss. The BNO film changed from a gel to a solid at this temperature. A small endothermic peak was also observed at approximately 550 °C owing to crystallization of the BNO film from an amorphous phase to cubic pyrochlore microcrystals (discussed below).

Figure 2 presents the relative dielectric constant and $\tan\delta$ in the BNO films as a function of the annealing temperature. In this experiment, the total annealing time was fixed at 40 min. From 515 °C to 550 °C, the relative dielectric constant increased with increasing annealing temperature, reaching a maximum value of $\simeq$140 at 550 °C. The relative dielectric constant then decreased as the annealing temperature was further increased and ultimately was saturated at values below 60. The $\tan\delta$ values were below 0.02, and the leakage current densities were below 1×10^{-7} A/cm^2 at 0.3 MV/cm for all samples, indicating that the calculated relative dielectric constants were intrinsic. On the other hand, the relative dielectric constants of BNO films deposited via sputtering were found to be approximately 43 (Refs. 11 and 12) and varied only slightly with annealing temperature.[8] Therefore, the deposition method (solution process vs. sputtering) significantly affected the properties of the BNO films.

Figure 3 shows the results of XRD analyses of the BNO films annealed at various temperatures. These BNO films were spin-coated onto the Pt substrates and annealed for 40 min, which corresponded to the total annealing time for the standard process. From 250 °C to 500 °C, no crystalline

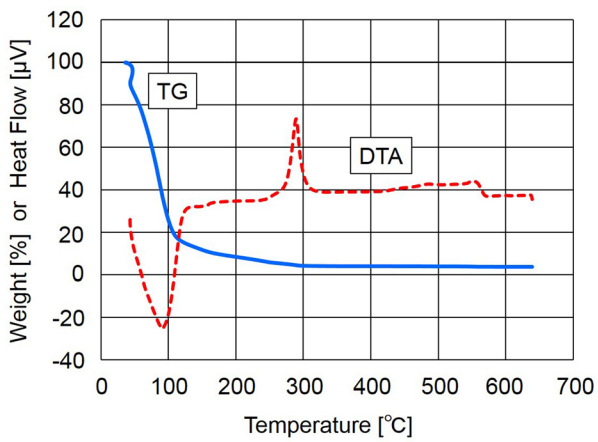

FIG. 1. TG-DTA analysis results for the BNO precursor solution.

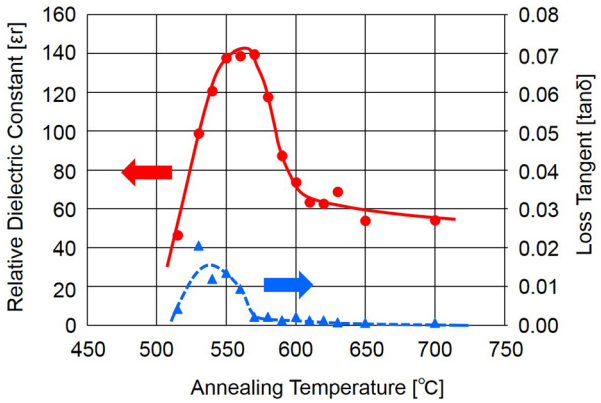

FIG. 2. Relative dielectric constants of the BNO films as a function of the annealing temperature. The standard deviation (σ) of the relative dielectric constant values for the BNO film annealed at 550 °C was 5.17.

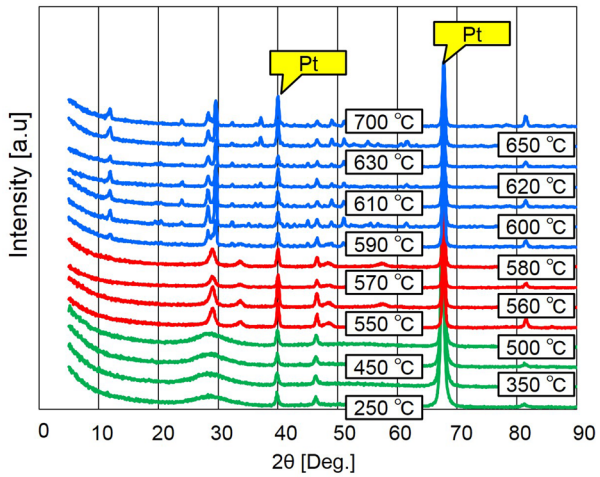

FIG. 3. XRD patterns for the BNO films annealed at various temperatures.

diffraction peaks were observed, indicating that these BNO films were amorphous. However, a crystalline diffraction peak appeared at $2\theta \simeq 29°$ for the BNO film annealed at 550 °C. Two additional peaks also appeared at $2\theta \simeq 28°$ and 30° in the XRD pattern of the BNO film annealed at 590 °C, which were attributed to the appearance of a second crystalline structure.

Figures 4(a) and 4(b) show the cross-sectional HRTEM images of the BNO film fabricated using the standard process (O_2/550 °C/40 min). Microcrystals with diameters of several tens of nanometers were observed. This BNO film was found to consist of three phases depending on the NBD analysis. Figure 5(a) shows the NBD pattern for area A in Figure 4(a). No clear diffraction pattern was observed, indicating that this area was an amorphous phase. Figures 5(b) and 5(c) show the NBD patterns at areas B and C in Figure 4(b), respectively. The NBD pattern for area B agreed with the simulation data for crystalline Bi_3NbO_7, which has a fluorite structure,[13,14] as shown in Figure 5(d). Bi_3NbO_7 crystals are reported have two crystal structures—cubic and tetragonal—with relative dielectric constants of approximately 100 and 90, respectively. In area C, the NBD pattern was not consistent with simulation data for the BiNbO structure reported to date. However, it did correspond with the simulation data for $(Bi_{1.5}Zn_{0.5})(Nb_{1.5}Zn_{0.5})O_7$ with a cubic pyrochlore structure,[15] as shown in Figure 5(e), despite the fact that the BNO film did not contain Zn. From this result, we concluded that this BNO film had a cubic pyrochlore structure. In addition, the EDX analysis clarified that the ratio of Bi to Nb was 43.2 to 56.8 in this cubic pyrochlore BNO microcrystal. The composition of the cubic pyrochlore is $A_2B_2O_7$, i.e., Bi/Nb = 1. Therefore, Bi deficits were formed in the cubic pyrochlore BNO microcrystal, i.e., $Bi_xNb_2O_7$ ($x < 2$), for the BNO films deposited via a solution process. Note that phase separation of the bismuth oxide was not observed according to the results of the TEM, SAED, and NBD analyses.

The XRD pattern for the BNO film annealed using the standard process (O_2/550 °C/40 min) was deconvoluted into the three phases (amorphous, Bi_3NbO_7 fluorite microcrystal, BNO cubic pyrochlore microcrystal). The crystallinity was then determined from the deconvolution results. The ratio of the BNO cubic pyrochlore microcrystal and Bi_3NbO_7 fluorite microcrystal was also determined using the reference intensity ratio method. Here, the data for the $(Bi_{1.5}Zn_{0.5})(Nb_{1.5}Zn_{0.5})O_7$ cubic pyrochlore structure were utilized for those of the BNO cubic pyrochlore structure. From these analyses, we estimated that the crystallinity was 82.6% and the ratio of Bi_3NbO_7 fluorite microcrystal to BNO cubic pyrochlore microcrystal was 36.3% to 63.7%. Consequently, the proportions of the amorphous, Bi_3NbO_7 fluorite microcrystal, and BNO cubic pyrochlore microcrystal phases were 17.4%, 30.0%, and 52.6%, respectively, as shown in Table I. Note that the BNO cubic pyrochlore microcrystal was a major phase in the BNO film, which suggests that the high

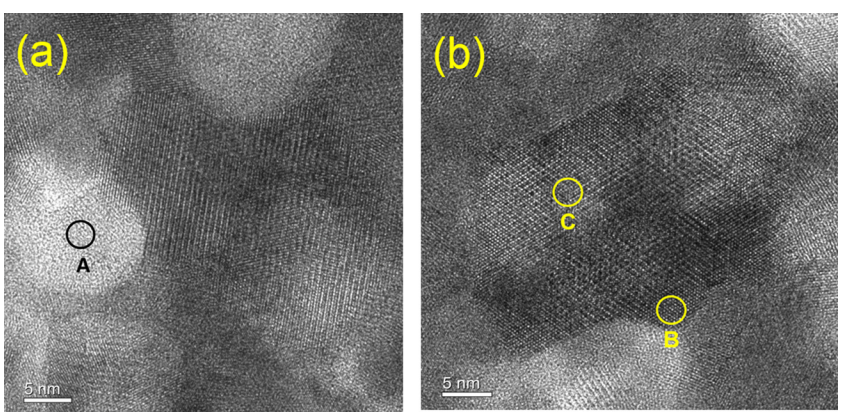

FIG. 4. Cross-sectional HRTEM images of the BNO film fabricated using the standard process (O_2/550 °C/40 min).

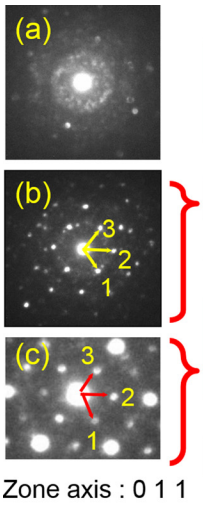

(d)

Bi_3NbO_7	Measurement Results of NBD (b)	Simulation Data
$d_{1\,1\,-1}$	0.317	0.316
$d_{2\,0\,0}$	0.273	0.273
$d_{1\,-1\,1}$	0.317	0.311

(e)

$(Bi_{1.5}Zn_{0.5})(Nb_{1.5}Zn_{0.5})O_7$	Measurement Results of NBD (c)	Simulation Data
$d_{1\,1\,-1}$	0.610	0.612
$d_{2\,0\,0}$	0.528	0.532
$d_{1\,-1\,1}$	0.610	0.616

FIG. 5. NBD patterns and a comparison of the experimentally determined lattice constants with those in the simulation data. (a) NBD pattern for area A in Figure 4(a), (b) NBD pattern for area B in Figure 4(b), (c) NBD pattern for area C in Figure 4(b), (d) comparison of the lattice constants for crystalline Bi_3NbO_7, and (e) comparison of the lattice constants for $(Bi_{1.5}Zn_{0.5})(Nb_{1.5}Zn_{0.5})O_7$ cubic pyrochlore crystal.

dielectric constant can be attributed to the existence of the BNO cubic pyrochlore microcrystals.

Figures 6(a) and 6(b) show the cross-sectional HRTEM images of a BNO film annealed at 600 °C for 20 min under O_2. Crystals with diameters of several hundreds of nanometers were observed in the BNO film. Figures 7(a) and 7(b), respectively, show the SAED patterns at areas D and E in Figure 6. The SAED pattern at area D agreed with the simulation data for the $(Bi_{1.5}Zn_{0.5})(Nb_{1.5}Zn_{0.5})O_7$ cubic pyrochlore microcrystal, as shown in Figure 7(c). On the other hand, the SAED pattern at area E agreed with the simulation data for β-$BiNbO_4$ with a triclinic crystal structure,[16–20] as shown in Figure 7(d).

As discussed above, the relative dielectric constant decreased to below 100 for the BNO film annealed at 600 °C. Consequently, we inferred that the relative dielectric constant for the β-$BiNbO_4$ crystal was lower than that of the BNO cubic pyrochlore microcrystal. To verify this hypothesis, the BNO film annealed at 600 °C for 20 min under O_2 was analyzed using the SNDM method. In this analysis, it was difficult to obtain an accurate dielectric constant for the BNO film; however, a qualitative comparison of the β-$BiNbO_4$ crystals and the other areas of the BNO film were possible. The BNO film fabricated under these annealing conditions was found to consist of large triclinic β-$BiNbO_4$ crystals, as shown in Figure 6(b), which was also observed in the AFM image shown in Figure 8(a). As can be seen in Figure 8(b), the SNDM image corresponded to the AFM image, indicating that the dielectric constant of the triclinic β-$BiNbO_4$ crystals was lower than that of area D in Figure 6.

The temperature coefficient of a BNO capacitor fabricated using the standard process (O_2/550 °C/40 min) was determined to be −332 ppm/°C, and that of a BNO capacitor annealed at 600 °C under O_2 (total annealing time: 40 min) was 148 ppm/°C. These results indicate that the temperature coefficient was negative for the BNO cubic pyrochlore microcrystalline film and positive for the triclinic β-$BiNbO_4$ crystalline film. Therefore, it is possible to reduce the temperature coefficient of a capacitor using a BNO film that is composed of a mixture of cubic pyrochlore microcrystals and triclinic β-$BiNbO_4$ crystals. Details of the temperature coefficient of the BNO capacitors will be discussed elsewhere.

TABLE I. Proportions of the amorphous phase, cubic pyrochlore microcrystals, and Bi_3NbO_7 fluorite microcrystals in the BNO film annealed at 550 °C.

Amorphous	Bi_3NbO_7	Pyrochlore
	82.6% (Crystallinity)	
17.4%	30.0%	52.6%

Next, TDS analysis of the BNO gel was performed to verify the mechanism of formation of the cubic pyrochlore structure for the solution-processed BNO films. The desorbed molecules included CO_2, CO, H_2O, H_2, and C_2H_2, and several peaks were detected, as shown in Figure 9. Two clear peaks observed at approximately 440 °C and 530 °C were attributed to CO_2 and CO. An H_2O peak was also observed along with the first CO_2/CO peak at 440 °C, indicating that CO_2/CO desorption can be explained by the thermal decomposition of a hydrocarbon. On the other hand, no H_2O peak was observed with the second CO_2/CO at 530 °C. Therefore, this CO_2/CO desorption event was attributed to the thermal decomposition of carbon combined with a metal and/or oxygen, such as an M-O-C-M bond. Notably, the temperature at which the second CO_2/CO peak appeared was nearly consistent with that associated with the appearance of the cubic pyrochlore structure. Table II lists the atomic concentrations for oxygen, hydrogen, and carbon in BNO films annealed at 450 °C/8 h, 500 °C/20 min, and 550 °C/20 min. The carbon concentration decreased as the annealing temperature increased; however, the BNO films contained 6.5 atm. % carbon even after annealing at 500 °C. This level dropped to below 1.3 atm. % in the BNO film annealed at 550 °C, which was the lower limit of measurement, indicating that the carbon was released from the BNO film at this temperature.

Based on the results described above, a hypothesis for the formation and crystallization of the BNO films fabricated via spin coating was proposed and is presented in Figure 10. After spin coating, the BNO solution changes to the gel state during the drying process at 250 °C. The gel film is then pyrolyzed at approximately 290 °C and converted to a solid film (amorphous phase) at this temperature. Solution-processed BNO films contain a lot of carbon attributed to

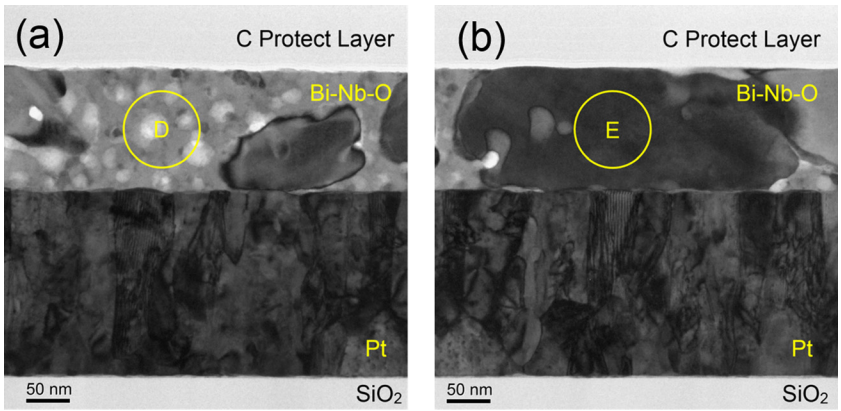

FIG. 6. Cross-sectional HRTEM images of the BNO film annealed at 600 °C for 20 min under O_2.

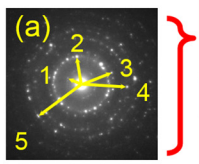

(c)

$(Bi_{1.5}Zn_{0.5})(Nb_{1.5}Zn_{0.5})O_7$	Measurement Results of SAED (a)	Simulation Data
$d_{1\,1\,1}$	0.604	0.609
$d_{2\,2\,2}$	0.306	0.305
$d_{4\,0\,0}$	0.263	0.264
$d_{4\,4\,0}$	0.185	0.187
$d_{6\,2\,2}$	0.160	0.159

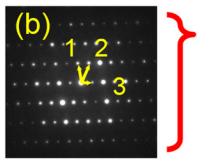

Zone axis : 1 1 0

(d)

β-$BiNbO_4$	Measurement Results of SAED (b)	Simulation Data
$d_{1\,-1\,0}$	0.305	0.305
$d_{1\,-1\,1}$	0.265	0.264
$d_{0\,0\,1}$	0.307	0.305

FIG. 7. SAED patterns and a comparison of the experimentally determined lattice constants with those in the simulation data. (a) SAED pattern for area D in Figure 6, (b) SAED pattern for area E in Figure 6, (c) comparison of the lattice constants for $(Bi_{1.5}Zn_{0.5})(Nb_{1.5}Zn_{0.5})O_7$ cubic pyrochlore crystal, and (d) comparison of the lattice constants for β-$BiNbO_4$ triclinic crystal.

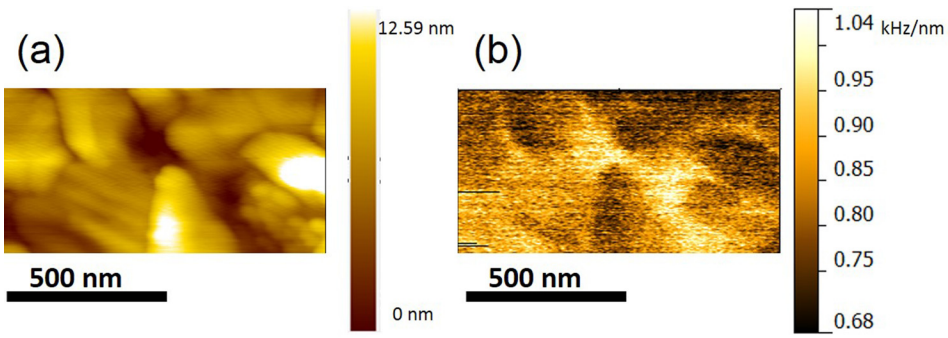

FIG. 8. (a) AFM and (b) SNDM images of the BNO film annealed at 550 °C.

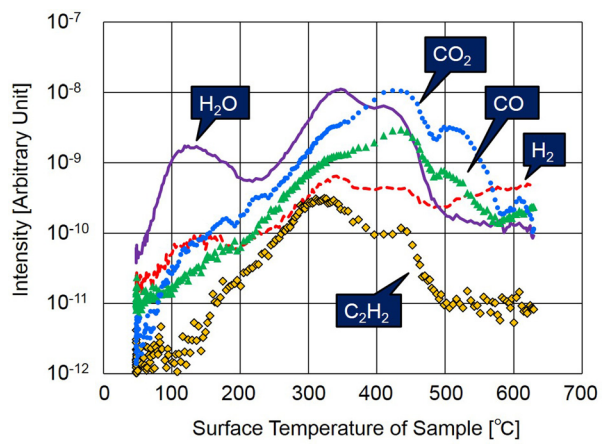

FIG. 9. Result of the TDS analysis of the BNO gel.

Bi-2EH and Nb-2EH, which suppresses crystallization up to 500 °C, resulting in a new crystallization path. Crystallization begins immediately after desorption of carbon. Initially, cubic pyrochlore crystals are formed as a transient phase, and subsequently, the stable phase (triclinic β-$BiNbO_4$ crystal) is formed at approximately 590 °C.

TABLE II. Atomic concentrations of oxygen, hydrogen, and carbon in BNO films annealed under varying conditions in an O_2 atmosphere.

	Oxygen atm. %	Hydrogen atm. %	Carbon atm. %
450 °C/8 h	49.0	14.1	11.2
500 °C/20 min	55.7	7.8	6.5
550 °C/20 min	64.9	<0.7	<1.3

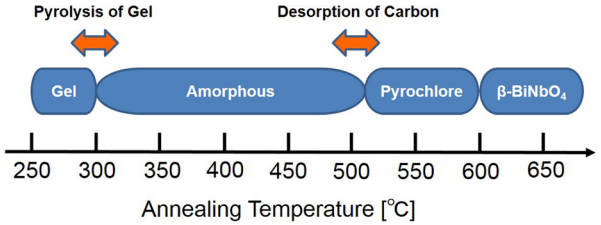

FIG. 10. Crystallization pathway for BNO films fabricated using a solution process.

Currently, it is unclear why carbon suppresses crystallization and why the cubic pyrochlore crystal is formed after desorption of carbon. Further studies are underway to establish a hypothesis that can explain this behavior.

IV. SUMMARY

The characteristics of the BNO films deposited using a solution process were investigated. When the BNO film was annealed at 550 °C for 40 min under an O_2 atmosphere, the relative dielectric constant was 140, which was over three times higher than that of BNO films deposited using a sputtering method. Analysis of the film morphology revealed the presence of cubic pyrochlore microcrystals in the film, which has not been previously observed. The appearance of the cubic pyrochlore structure results in the high relative dielectric constant. It is thought that carbon in the BNO films suppresses crystallization and leads to a new crystallization pathway, which results in the appearance of the cubic pyrochlore structure. This result therefore suggests the capability to design new materials using solution processes. The unique features of the BNO films obtained using the solution process make them attractive as dielectric films in capacitors and insulators for thin-film transistors.[21]

ACKNOWLEDGMENTS

The authors would like to thank Mr. Kosuke Ajisaka and the members of the Green Device Research Center, Japan Advanced Institute of Science and Technology (JAIST) and/or JST-ERATO Shimoda Nano-Liquid Process Project for their support of this study. This work was supported by the ERATO project of the Japan Science and Technology Agency (JST).

[1]T. Shimoda, Y. Matsuki, M. Furusawa, T. Aoki, I. Yudasaka, H. Tanaka, H. Iwasawa, D. Wang, M. Miyasaka, and Y. Takeuchi, Nature **440**, 783 (2006).
[2]P. F. Moonen, I. Yakimets, and J. Huskens, Adv. Mater. **24**, 5526 (2012).
[3]D. H. Lee, Y. J. Chang, G. S. Herman, and C. H. Chang, Adv. Mater. **19**, 843 (2007).
[4]M. Klee, D. Wissen, W. Keur, R. Kiewitt, D. Bausen, and P. Lok, in *Oxide Films for Integrated Capacitors in Thin Film Functional Modules*, edited by S. R. Gilbert, M. Miyasaka, R. W. Schwartz, and D. Wouters (Mater. Res. Soc. Symp. Proc., 2000), Vol. 655, p. CC13.1.1.
[5]W. Ren, S. Trolier-McKinstry, C. A. Randall, and T. R. Shrout, J. Appl. Phys. **89**, 767 (2001).
[6]R. L. Thayer, C. A. Randall, and S. Trolier-McKinstry, J. Appl. Phys. **94**, 1941 (2003).
[7]N. Wang, M. Y. Zhao, Z. W. Yin, and W. Li, Mater. Lett. **57**, 4009 (2003).
[8]M. Onoue, T. Miyasako, E. Tokumitsu, and T. Shimoda, IEICE Electron. Express **11**, 20140651 (2014).
[9]K. Ohara and Y. Cho, Jpn. J. Appl. Phys., Part 1 **41**, 4961 (2002).
[10]T. Kaneda, D. Hirose, T. Miyasako, P. T. Tue, Y. Murakami, S. Kohara, J. Li, T. Mitani, E. Tokumitsu, and T. Shimoda, J. Mater. Chem. C **2**, 40 (2014).
[11]H. Lim and Y.-J. Oh, Jpn. J. Appl. Phys., Part 1 **45**, 5865 (2006).
[12]D. Zhou, H. Wang, X. Yao, X. Wei, F. Xiang, and L. Pang, Appl. Phys. Lett. **90**, 172910 (2007).
[13]U. Pirnat, M. Valant, B. Jancar, and D. Suvorov, Chem. Mater. **17**, 5155 (2005).
[14]M. Valant, B. Jancar, U. Pirnat, and D. Suvorov, J. Eur. Ceram. Soc. **25**, 2829 (2005).
[15]J. Lu, D. O. Klenov, and S. Stemmer, Appl. Phys. Lett. **84**, 957 (2004).
[16]H. Kagata, T. Inoue, J. Kato, and I. Kameyama, Jpn. J. Appl. Phys., Part 1 **31**, 3152 (1992).
[17]S. Butee, A. J. Kulkarni, O. Prakash, R. P. R. C. Aiyar, K. Sudheendran, and K. C. J. Raju, J. Alloys Compd. **492**, 351 (2010).
[18]E. S. Kim and W. Choi, J. Eur. Ceram. Soc. **26**, 1761 (2006).
[19]N. Wang, M. Y. Zhao, W. Li, and Z. W. Yin, Ceram. Int. **30**, 1017 (2004).
[20]M. H. Weng and C. L. Huang, J. Mater. Sci. Lett. **19**, 375 (2000).
[21]T. Miyasako, M. Onoue, E. Tokumitsu, and T. Shimoda, in *2011 MRS Fall Meeting, Abstract S2.8, 28 November-2 December, Boston, USA*, see http://www.mrs.org/f11-abstracts-s/.